Investigating Anomalous Growth of Platinum Particles during Accelerated Aging of Diesel Oxidation Catalysts

Deepak Kunwar[1], Cristhian Carrillo[1], Haifeng Xiong[1], Eric Peterson[1], Andrew DeLaRiva[1], Arnab Ghosh[1], Gongshin Qi[2], Ming Yang[2], Michelle Wiebenga[2], Se Oh[2], Wei Li[2] and Abhaya K. Datye[1]*

[1]Department of Chemical & Biological Engineering and Center for Microengineered Materials, University of New Mexico, Albuquerque, NM 87131 (USA)

[2]General Motors Global Research and Development, Chemical and Materials Systems Lab, Warren, MI 48090, (USA)

*datye@unm.edu

Keywords

Sintering of Pt, Volatilization of Pt, Diesel Oxidation Catalysts, Trapping of Pt atoms, CO oxidation

Abstract

When Pt catalysts are aged in air at 800 °C, we see significant growth of Pt particle sizes. The particle size distributions in the aged catalysts are usually bimodal, with some very large particles coexisting with smaller particles. Here we investigate the origins of these anomalous particle size distributions and relate them to the vapor phase transport of PtO_2 under oxidizing conditions. Our results suggest that the emission of PtO_2 from the catalyst into vapor phase could be a cause for the anomalous growth of Pt particles observed during high temperature aging. We show that supports such as ceria that can trap Pt ions cause a suppression of vapor phase transport, while the alumina and the $MgAl_2O_4$ spinel supports are unable to trap the Pt ions leading to the formation of abnormally large Pt particles.

Introduction

The USDRIVE Low Temperature aftertreatment (LTAT) test protocol requires aging of diesel oxidation catalysts at 800 ˚C [1]. This high temperature treatment for 50 hours simulates the

degradation experienced by Pt catalysts after 150K miles of driving. The catalysts lose activity due to formation of large particles and the attendant decrease in metal surface area [2]. It is extremely important to stabilize the catalytically active Pt sites on support in order to extend the life-time of working catalysts and to make efficient use of the limited global availability of Pt. Harris et al. [3] were among the first to recognize that 'anomalously' large Pt particles were formed on Pt/Al_2O_3 catalyst after aging in air at 600 ˚C. Wynblatt [4] also reported the formation of 'abnormally large' Pt particles when the catalyst was aged at 20 kPa of oxygen during aging at 800 ˚C. Such large particles were not observed when the aging was performed at 2 kPa of oxygen. The mechanism for the formation of such large Pt particles is still under debate. Wynblatt [4] suggested that a morphological instability was responsible for forming large particles. Harris et al. [3] suggested that the particle growth mechanism during the first 2 hours of aging was interparticle transport, but no explanation was proposed for the 'anomalously large particles.' Graham et al. [2] reported that the anomalously large particles seen on the Pt only catalysts were not seen in any of the Pd containing catalysts.

At 800 ˚C in air Pt reacts with oxygen to form volatile PtO_2 [5]. The vapor pressure in equilibrium with Pt is 1.6×10^{-8} atm which facilitates the transport of Pt [5]. In previous work [6] we reported the transport of Pt from a Pt/La-alumina to physically mixed ceria particles leading to the formation of atomically dispersed Pt^{2+} species. A similar transport of Pt was found from $Pt/MgAl_2O_4$ to physically mixed PdO/La-alumina particles, forming Pt-Pd metallic nanoparticles [7]. The added Pd lowers the vapor pressure of Pt due to the solid solution, explaining in part the beneficial effect on particle size seen by Graham et al [2]. In previous work we demonstrated that lowering the oxygen pressure during catalyst aging at 800 ˚C also led to decreased particle size of Pt in the final catalyst [8]. All these observations suggest the formation and transport of PtO_2 vapor may play an important role in the formation of large Pt particles. To investigate this phenomenon further, we developed a model catalyst where the emission of Pt from catalyst powders could be quantified. We show that emission of Pt is rapid at 800 ˚C leading to loss of Pt if the catalyst is spread as a thin film on a surface over which air is allowed to flow. On the other hand, when air flows over a deep bed of catalyst, we do not see any loss of Pt. This is because the PtO_2 that would be emitted from individual catalyst grains in a thin film is trapped within the deep bed and deposits on the support forming anomalously large Pt particles. We show also how the catalyst support plays a critical role in modifying the emission of Pt and the resulting formation of large Pt particles.

In this work we studied La-Al_2O_3, $MgAl_2O_4$ and CeO_2 supports. La-Al_2O_3 is the most commonly used support in automotive exhaust emission control catalyst. CeO_2 is commonly added to three-way catalysts to provide oxygen storage capabilities [9]. $MgAl_2O_4$ was used because it is thermally stable and has been reported to stabilize small nanoparticles of Pt ranging from 1–3nm [10] at elevated temperature. The goal of this work was to develop a method to quantify the emission of volatile Pt species from industrially relevant catalysts. The vapor pressure of Pt is a thermodynamic quantity which can only be changed by alloying with other elements such as Pd, which have very low vapor pressure in oxygen. Since catalyst supports are known to modify the stability of Pt nanoparticles, the question remains whether the volatility of Pt can be influenced by the support. This study investigates the factors that lead to formation of anomalously large Pt particles during the accelerated aging of diesel oxidation catalysts. Such large Pt particles represent a waste of a precious resource and understanding the origin of this phenomenon can help to avoid formation of large Pt particles.

2. Experimental Details

2.1 Catalyst preparation and aging

Lanthanum stabilized alumina (La-Al_2O_3) support (MI-386) was obtained from SOLVAY Rhodia and contained ~5 wt% La_2O_3, with a BET surface area of 176 $m^2\ g^{-1}$. The particle size is 1-10 µm based on TEM images, the pore volume is 0.76 cm^3/g and particle density 0.48 g/cm^3 as reported previously by Wang et al [11]. The BET surface area before and after 800 ˚C extended aging for the three supports is reported in Table 1. Magnesium aluminate ($MgAl_2O_4$), cerium nitrate hexahydrate (99.999% purity) and tetraamine platinum nitrate were purchased from Sigma Aldrich. Cerium nitrate hexahydrate was heated in a box furnace at 350 ˚C for 4 hours in order to make polyhedral ceria (CeO_2). 1wt% Pt was loaded on $MgAl_2O_4$, La-Al_2O_3 and CeO_2 using incipient wetness impregnation and evaporated to dryness at 80˚C. The dried catalysts were calcined at 500 ˚C/4 hours, 550 ˚C/4 hours and 800 ˚C/10 hours, respectively, in flowing air in order to generate the initial catalyst. The higher temperature used for preparation of the ceria catalyst ensures that the Pt is atomically dispersed in the form of Pt^{2+} ions covalently bonded to the ceria support.

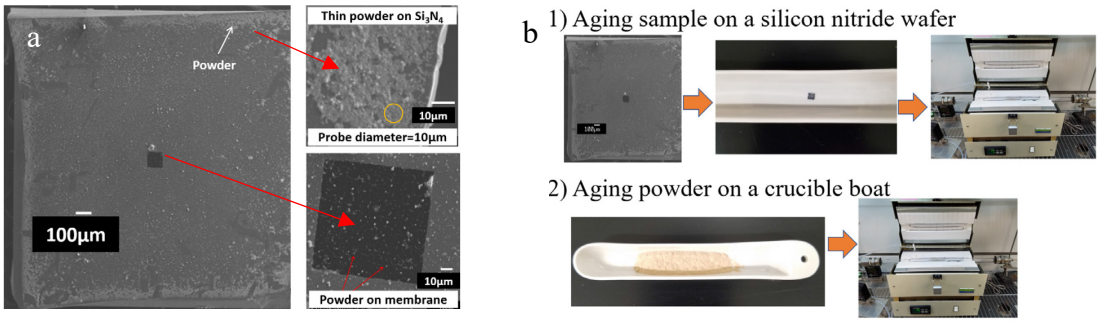

Fig. 1 (a) The model catalyst consists of a silicon wafer with a silicon nitride surface layer. A square window (100×100µm) creates an electron transparent silicon nitride film which allows TEM imaging and a typical region analyzed via SEM is shown and (b) The experimental approaches for aging the catalyst powder: as a thin layer dispersed on silicon nitride film (b1) and as a powder in a deep bed in a ceramic crucible (b2).

A small amount of the initial catalyst was dispersed in ethanol and mounted using a pipette on the TEM sample and spin coated to make a thin film shown in Figure 1. We estimate that the amount of sample placed on the silicon nitride grid is 0.035 mg. This estimate assumes that ~1mg of the catalyst powder was dispersed in 1.0 ml of ethanol and 1 drop of the suspension was deposited on the TEM sample. As described later, by using such a small amount of sample we increase the sensitivity to detect the changes on Pt content due to emission to the vapor phase. The method for fabricating the TEM samples was described in detail in our previous work [8]. SEM images of the catalyst powder in the form of a thin film are shown in Figure 1a at differing magnifications. The square window at the center of the TEM sample allows imaging through the Si_3N_4 thin film. Two approaches were used for aging the powder catalyst. First, as a thin film on the TEM silicon nitride sample as shown in Figure 1(b1) and second, using 500 mg of catalyst in a ceramic crucible boat as shown in Figure 1(b2). In both cases, the samples were placed in a quartz tube and treated at 800 ˚C for differing lengths of time in 100 cc/min of flowing air to generate the aged catalysts.

3. Characterization

After aging the powder catalysts on a silicon nitride surface at 800 ˚C, we determined the content of Pt using Scanning Electron Microscopy Energy Dispersive Spectroscopy (SEM-EDS), Wavelength Dispersive X-ray Spectroscopy (WDS) in an Electron Probe Microanalyzer (EPMA) and Transmission Electron Microscopy Energy Dispersive Spectroscopy (TEM-EDS). A typical

region analyzed by SEM and TEM is shown in Fig. 1a. A total of 15 such regions were analyzed by SEM-EDS and TEM-EDS for Pt quantification. The average of these analyses was reported to determine the loss of Pt after each heat treatment. We also used ICP-OES to analyze the elemental composition of the crucible-aged $Pt/MgAl_2O_4$ sample. High resolution transmission electron microcopy was carried out using a JEOL 2010F microscope. The catalyst was ground in a mortar and pestle and deposited on holey carbon support films after being dispersed in ethanol. Powder X-Ray diffraction (XRD) patterns were recorded with a Rigaku Smart Lab diffractometer using Cu Kα radiation and a Ni filter. XRD was also used to quantify the amount of crystalline Pt via Rietveld Refinement. CO oxidation was chosen as a probe reaction. Reaction rate measurements were performed using ¼ inch diameter U-tube with 20 mg of sample. The gas flow rates for CO oxidation were: CO 1.5 ml/min, O_2 1 ml/min and He 75 ml/min (space velocity 232,500 ml/g/h). The products were analyzed by a Varian CP-4900 Micro GC while the reactor temperature was ramped up at 2 °C/min. A Micromeritics AutoChem 2920 instrument was employed for the CO chemisorption in order to determine Pt dispersion. 100 mg sample was measured and placed in a sample tube for each experiment. The sample was first treated in a mixture of 10% O_2/He for 1 hour at 350˚C, then treated with 10% H_2/Ar for half an hour at 350˚C. Helium was allowed to flow to the catalyst with the flow rate of 50 ml/min for 30 min in order to stabilize the catalyst temperature to 45 ˚C. The 10% CO/He pulses were injected into the sample tube to start the chemisorption measurement, and a TCD detector recorded the concentration signals. The CO-Pt adsorption ratio was assumed to be 1:1.

4. Results and Discussion

4.1 Aging of Pt catalyst in the form of a thin film

The thin film geometry is designed to mimic the external surface of a wash coat in a honeycomb monolith used in a catalytic converter. We would expect that Pt emitted from the catalyst would be carried away in the flowing air and would lead to a decrease in the concentration of Pt. The initial samples, as-prepared and calcined, were found to contain ~1 wt% Pt via SEM-EDS, close to the nominal loading. STEM images of $Pt/La\text{-}Al_2O_3$ and $Pt/MgAl_2O_4$, Figure 2 (a, b), show small and well dispersed Pt nanoparticles in the initial catalyst, with the alumina having smaller particles than the spinel. More images are shown in supporting information (Figures S1 and S2). After aging the catalysts at 800 ˚C for 30 hours no Pt nanoparticles were observed, as shown in Fig. 2(e, f)

suggesting that all the Pt evaporated from the catalysts in the form of volatile PtO_2 after 30 hours of aging. This observation of Pt loss is consistent with the observations by Porsgaard et al. [12] who heated their samples up to 600 ˚C in 0.5 Torr of oxygen and observed 50% loss of Pt. Likewise, Fryburg and Petrus [13] measured the transport of Pt from a heated ribbon in the presence of oxygen to the cold walls of their glass apparatus. They reported that with increasing pressure, the PtO_2 emitted from the surface collides with gas phase molecules and a fraction will return back to the surface. The fraction lost decreased from 1.0 at low pressures to 0.006 at an oxygen pressure of 15×10^{-6} Torr. If we extrapolate to the pressures used in our study (21% oxygen, 630 Torr total pressure) we can see that the rate of Pt oxide emission can still be significant. In our experimental set up, once the PtO_2 is formed, it is swept away by flowing air. This explains why we see complete loss of Pt after 7 hours aging at 800˚C. To derive the time dependence of Pt, we studied the thin film samples via SEM-EDS (Figure 3a). The experimental error by SEM-EDS is within ± 15%. Elemental analysis was also performed via TEM-EDS and WDS to corroborate the SEM-EDS and the agreement was excellent.

We observed rapid loss of Pt from the Pt/La-Al_2O_3 and Pt/$MgAl_2O_4$ via SEM-EDS with almost all the Pt lost after 7 hours of aging at 800 ˚C in flowing air. The linear relationship between Pt content and time of aging is consistent with a constant vapor pressure of Pt regardless of the amount of Pt remaining in the sample. The similar rate of loss for both supports suggest a similar internal pore structure causing a similar resistance to mass transfer of the Pt species from the particles to the gas phase. For each sample, 15 regions were analyzed via SEM-EDS and the average of these measurements is shown in this figure. The amount of Pt left after aging for 7 hours on the Pt/$MgAl_2O_4$ and Pt/La-Al_2O_3 is close to the detection limit of this technique. If we assume that all of this Pt was vaporized and carried by the flowing gas, we would expect a gas phase concentration of Pt which is ~5% of saturation. The details are provided in table S1. In contrast, in the case of ceria, the entire amount of Pt was retained on the support without no detectable loss even after aging for 30 hours.

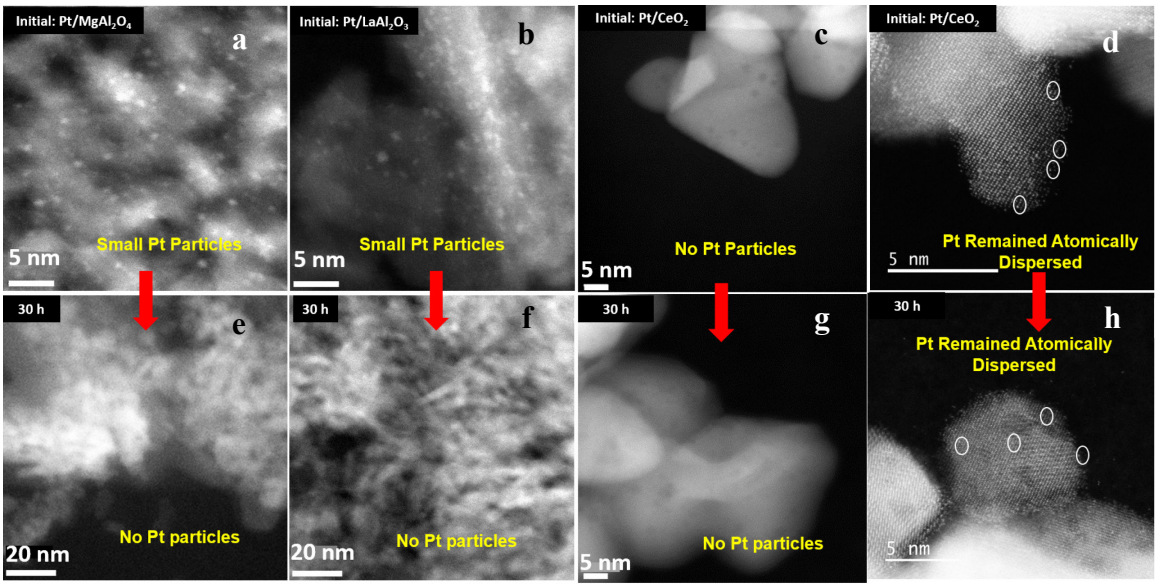

Figure 2. STEM images of (a–c) initial catalyst and (e–g) after aging for 30 h at 800 °C in flowing air on a thin film. Images d and h are AC-STEM images showing Pt single atoms.

Interestingly, we did not find any Pt particles in the STEM images on the ceria support both in the initial catalyst (which was already aged at 800 °C for 10 h during catalyst preparation) as well as after additional aging for 30 hours, as shown in Figure 2 (c, g). However, The EDS data shows the Pt content on the ceria support is unchanged after aging for 30 hours. Aberration corrected (AC) STEM images of the initial and the 30 hours aged sample show clearly resolved white dots corresponding to Pt atoms. Similar images have been reported in our previous work on ceria [6,13]. The atomically dispersed Pt was strongly bound to the step edges of ceria (111) as first shown by Dvorak et al [15]. The strong binding of Pt to ceria apparently prevents the evaporation of Pt which explains why the Pt content remained unchanged. The schematic in Figure 3 shows why the behavior of the ceria support is so different, since the oxidized Pt bound covalently to ceria does not further react with oxygen to form volatile species.

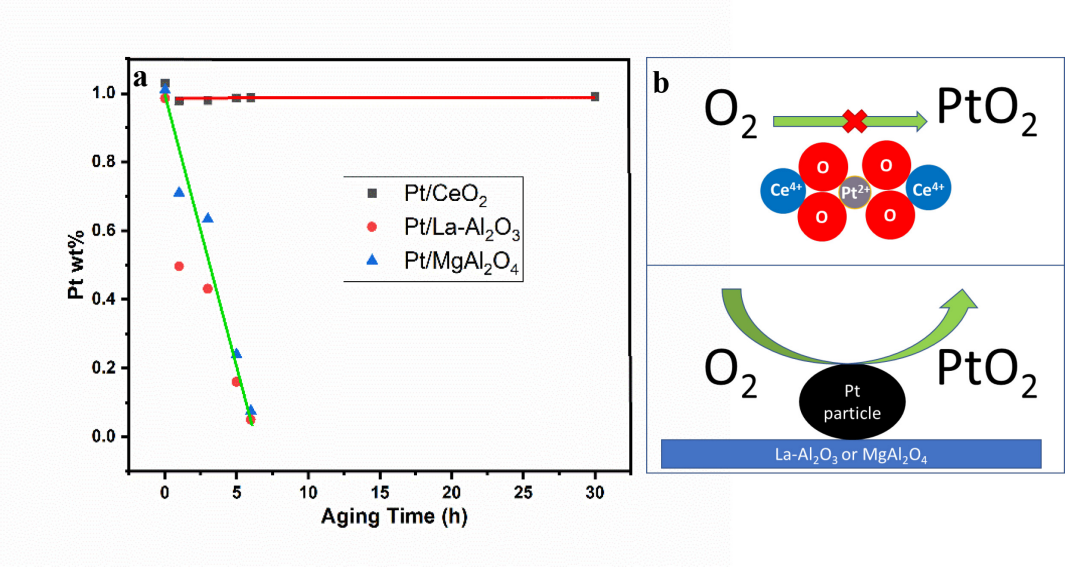

Figure 3. a) Pt content (via SEM-EDS) as a function of time (hours) after aging from catalyst thin films on model TEM sample and b) Schematic showing the different states of Pt on the ceria versus the La-Al_2O_3 and the $MgAl_2O_4$ supports.

The difference in the loss of Pt between the supports (Figure 3a) can be explained on the basis of the interaction chemistry between Pt and the support. Pt interacts with ceria through Pt-O-Ce bonds which cause the Pt to bind strongly to ceria [14,15,16]. While the stabilization of Pt by ceria was documented by Nagai et al [16], it was in the context of maintaining small Pt particle size. Here, we demonstrate, through the use of model catalysts, that ceria also helps to prevent the volatilization of Pt. Our work shows how volatilization of Pt can be related to the anomalous growth of Pt particles during aging, which the ceria helps to prevent. At ceria (111) step edges, Ce^{3+} ions are under coordinated and available to bind to PtO_2 species that are delivered through the gas phase, forming covalent bonds to form Ce^{4+} as illustrated in Figure 3b [14]. DFT calculations showed that Pt-CeO_2 interaction at step edges is very strong, with a Pt binding energy of 7.72 eV. We refer to the platinum as ionic because EXAFS and XPS are consistent with Pt^{2+} [14]. In analogy with the compound Platinum (II) bis (acetylacetonate) where the Pt has oxidation state +2 but the bonding to the ligand is covalent, we refer to Pt as being covalently bonded to the ceria through oxygen ligands. As shown in the schematic in Figure 3b, the trapped ionic Pt species do not react with oxygen and hence are stable during heating in air at 800 ˚C. However, a nanoparticle of Pt reacts with oxygen to form PtO_2, a process which is energetically uphill by 3.04 eV, but is feasible at the high temperature used for the aging. The reaction of Pt to form volatile

PtO_2, when supported on La-Al_2O_3 and $MgAl_2O_4$, causes the loss of Pt as shown in Figure 3a. The difference in emission rate on ceria and the other supports can be related to the different starting point. In the case of ceria, we start with Pt ions which were created through the method of atom trapping. These Pt ions being stable do not emit to the gas phase and we see no loss of Pt.

4.2 Aging of Pt catalyst in a ceramic crucible boat

Table 1 shows the BET surface areas of the three catalyst samples before and after 30 hours of aging in air. The spinel support lost 22% of its BET surface area after 30 hours of aging. In contrast the La-Al_2O_3 support was more stable, losing only about 7% of the initial surface area. The presence of La is known to stabilize alumina surface area. While ceria is known to lose surface area after aging, we have shown previously that atomically dispersed Pt helps to maintain BET surface area [6] due to the strong interaction between Pt and ceria [14]. In the case of the ceria sample, it had already been heated to 800 °C in air for 10 h during catalyst preparation.

Table 1: BET surface area of initial catalysts and aged (800˚C/30 h) catalysts.

Catalysts	BET surface area of initial catalysts (m^2/g)	BET surface area of aged catalysts (800 ˚C/30 h) m^2/g	BET surface area aged in steam (800 ˚C/4 h) m^2/g
1wt% Pt/CeO_2	32	30	-
1wt% Pt/La-Al_2O_3	190	178	160
1wt% $Pt/MgAl_2O_4$	142	110	80

The content of Pt in the initial catalysts was determined via TEM-EDS, WDS and SEM-EDS. Since the sample size for crucible aging was 500 mg, it was possible to perform more accurate elemental analysis. The $Pt/MgAl_2O_4$ initial and 30 hours aged samples were analyzed by Galbraith laboratories using ICP-OES. The initial catalyst had 1.1wt% Pt while it was 1.13wt% Pt after aging for 30 hours, indicating there was no loss of Pt into the vapor phase from the deep bed. If flowing gas was saturated in PtO_2 vapor, we would expect to lose ~0.58% of the initial amount of Pt in the sample, more details are provided in Table S1. This small decrease is below the detection limit of ICP-OES when the powder is aged in a crucible (sample depth of 3-5 mm). The surface of

the sample will lose Pt to the gas phase. By studying thin film samples, we were able to quantify the amount of Pt emitted via TEM or SEM-EDS. An alternative method for quantifying the emitted Pt is by capturing it down stream and measuring the ammonia oxidation activity, as shown by Leistner et al. [18]. This method is sensitive enough to detect Pt emission even when the catalyst temperature is 500˚C [18].

Figure 4 shows TEM images of the initial catalyst and after aging for 30 hours in a ceramic boat. The images of the initial catalysts were presented in Figure 2, so these images come from other regions of the sample to provide better statistics. The average Pt particle size in the initial catalyst is less than 1 nm. The TEM particle size distributions (PSD) for Pt/La-Al_2O_3 and Pt/$MgAl_2O_4$ are included in the supporting information and show that the average Pt particle size increases from less than 1 nm in the initial catalyst (Figures S1-S3) to 30 nm in the aged catalysts (Figures S4-S6). However, the average diameter derived from TEM images ignores the abnormally large particles which were also seen in these samples. The origin of these abnormally large particles will be discussed in detail in the next section. The presence of a few extremely large particles makes it very difficult to derive an average particle size for Pt in the 30 h aged catalysts. In contrast, the Pt/ceria catalyst does not show any Pt particles in TEM and SEM images of the initial catalyst as well as after aging. The Pt content on this catalyst is unchanged, and the Pt is only visible in AC-STEM images in the form of single atoms (Figure 4 d, h).

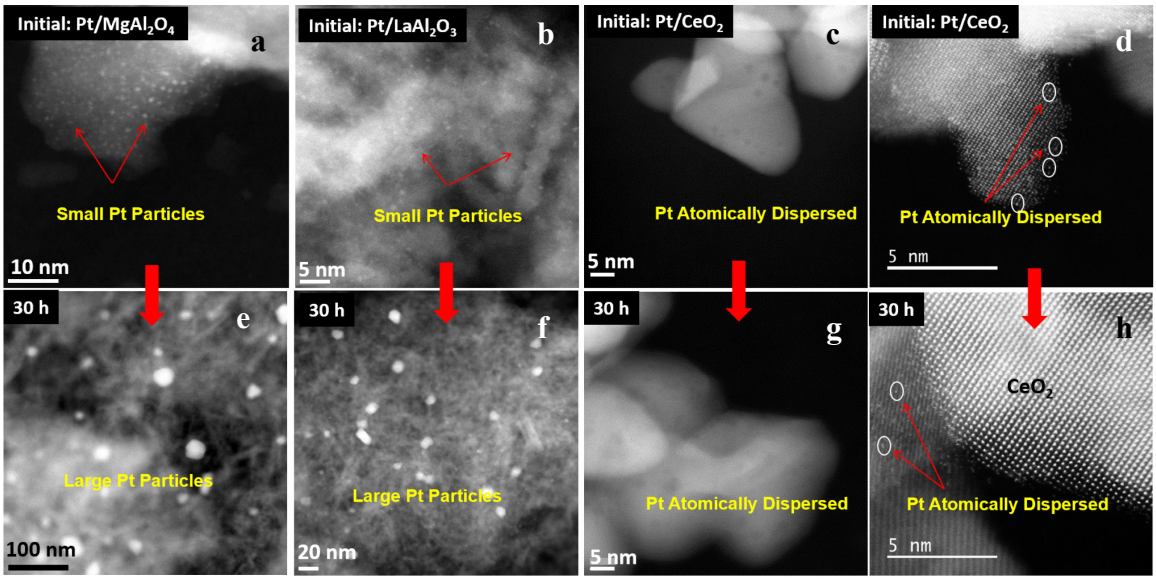

Figure 4. STEM images (a, b, c) of initial catalyst before aging and (e, f, g) after aging at 800 ˚C for 30 h in a crucible boat. AC-STEM images (d, h) of initial and aged catalyst.

The SEM images in Figure 5 show that the large particles are present after 30-hour aging on the La-Al_2O_3 and $MgAl_2O_4$ supports. These particles are located on the surface of the support, consistent with re-deposition of Pt that was emitted from within the support pore structure. The large particles range in size from 100 nm to greater than 1000 nm (Figure 5 and Figure S7), resulting in the sharp peaks seen via X-ray diffraction (Figure 6). Steam is present in all exhaust gases from combustion of hydrocarbons. It is known to accelerate catalyst sintering and deactivation. We also aged our samples in the presence of 10% steam and found that particle growth rates were enhanced. Some of the Pt particles grew larger than 10 microns when the 1wt%Pt/La-Al_2O_3 catalyst was aged at 800 ˚C for 4 hours in the presence of 10% steam (Figure S8). XRD analysis of the same catalyst shows a prominent Pt (111) peak (Figure S9) which yields an average particle size from the analysis of line broadening to be 58.4 nm without steam and 65 nm with steam. As shown in Figure 6, no Pt peak is seen via XRD for the Pt/Ceria catalyst. The content of metallic Pt was obtained from the areas of the XRD peaks using whole pattern fitting via the JADE program from MDI. Quantitative analysis of the XRD patterns shows that 0.8 wt% crystalline Pt was present on $Pt/MgAl_2O_4$, Pt/La-Al_2O_3 catalysts, suggesting that the remaining 0.2 wt% Pt may be in the form of small Pt particles and beyond the detection limit for XRD. The crystallite sizes of Pt reported for $Pt/MgAl_2O_4$, Pt/La-Al_2O_3 (without steam) and Pt/La-Al_2O_3 (with

steam) via XRD line broadening analysis were 39 nm, 58 nm and 65 nm respectively, as shown in Table 2. However, since SEM & STEM images show Pt particles range from 10 nm-2 µm in size without steam and up to 10 µm in size with steam, we do not think the XRD line broadening can provide an accurate average particles size, since the large particles will yield line width comparable to the instrumental line broadening.

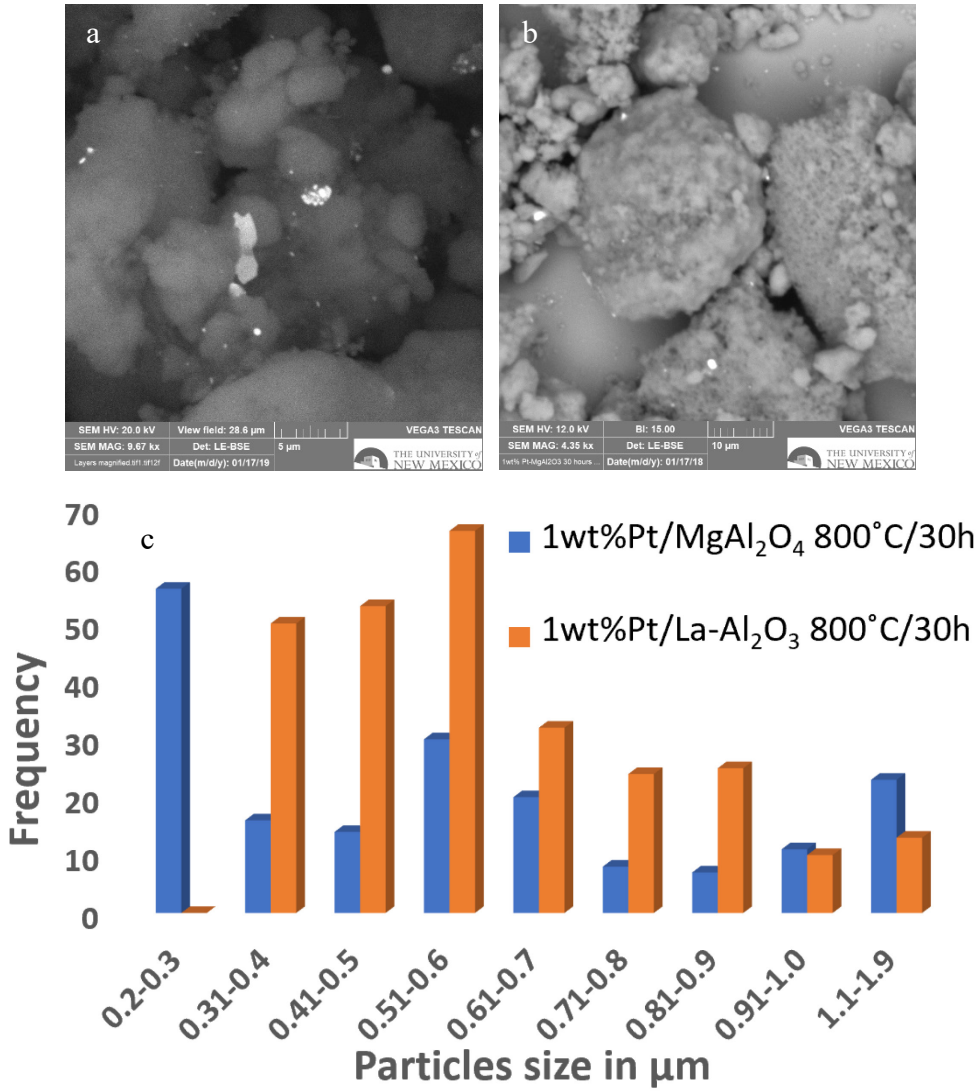

Figure 5. SEM image after aging at 800˚C/30 h a) 1wt%Pt/La-Al_2O_3 b) 1wt%Pt/$MgAl_2O_4$ and c) SEM particle size distribution for 800 ˚C/30 h aged catalysts

While XRD or TEM cannot provide an average particle size on these supports after aging, CO oxidation helps to show the impact of 800 ˚C aging on catalyst activity. The order of reactivity in

the initial catalyst was Pt/La-Al_2O_3 > Pt/$MgAl_2O_4$ > Pt/CeO_2 (Figure 7a). Pt/CeO_2 has lowest CO oxidation reactivity among these three catalysts because it contains ionic Pt which is not reactive for this reaction as shown in previous work [6,13]. Pt/La-Al_2O_3 showed higher activity than Pt/$MgAl_2O_4$ because it contains smaller Pt particles in its initial state (Figure S3). The dispersion of Pt on La-Al_2O_3 and $MgAl_2O_4$ on the initial catalysts via CO chemisorption was 50.8% and 18.6% respectively. We have included the TOF for these catalysts in the supporting information (Table S2 and Figure S10) and find these values to be consistent with the literature [11]. We ran three cycles of CO oxidation from room temperature up to 300 ˚C. We reported the third run in the manuscript (Figure 7a) but in the supporting information we have included all three runs (Figure S11, S12, S13). After aging the catalysts at 800 °C for 30 hours, the order of the reactivity becomes Pt/CeO_2 > Pt/$MgAl_2O_4$ ~ Pt/La-Al_2O_3 ~Pt/ La-Al_2O_3 (10% steam, 800 ˚C/4h). The formation of the large Pt particles explains the lower activity of spinel and alumina-supported catalysts shown in Figure 7b and Figure S4, S5, S6, S7, S8 and S9.

While there are some differences in the particle size distribution from SEM imaging (Figure 5), the surface area of metallic Pt after 30 hours aging is so low that CO oxidation reactivity is comparable to that of support (Figure S14). In contrast the reactivity of Pt/CeO_2 was unchanged after 30 hours aging. There is no agglomeration of Pt atoms to form nanoparticles, and a minor decrease in the BET surface area. In our DRIFTS observations performed *in situ* during CO oxidation, we found that the adsorbed CO was strongly bound. Switching off the flow of CO while allowing He to flow did not decrease the size of the CO peak at 125˚C [6] and this adsorbed CO could not be reacted with flowing oxygen at this temperature. This is the reason for the low reactivity of as-synthesized Pt/CeO_2 catalyst. When this catalyst was reduced in CO at 275 ˚C it became remarkably active for low temperature CO oxidation [17] due to facile oxygen transfer from the ceria support.

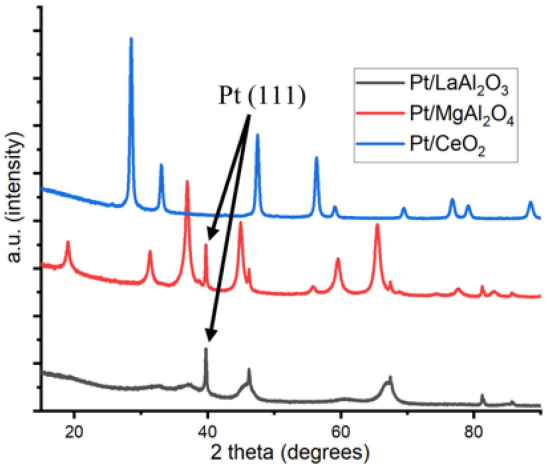

Figure 6. XRD patterns for the catalysts aged at 800 ˚C in air for 30 h in a crucible boat.

Table 2: XRD Characterization of catalyst-scale Pt powder catalysts after aging for 30 h at 800 ˚C. "n.d." indicates not detectable by XRD.

Pt Catalyst Support	Crystalline Pt (wt%)	Pt Crystallite Size (nm)
1 wt% Pt/CeO_2	n.d.	n.d.
1 wt% $Pt/MgAl_2O_4$	0.78	39.4
1 wt% $Pt/La\text{-}Al_2O_3$	0.76	58.4
1 wt% $Pt/La\text{-}Al_2O_3$ (steam)	0.81	65

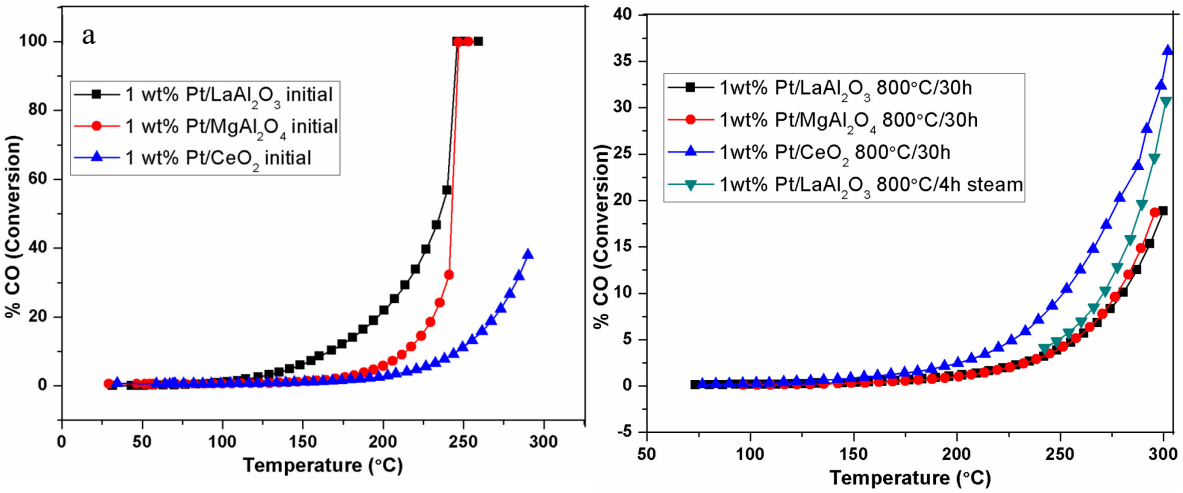

Figure 7. CO oxidation activity for the initial (a) and aged (b) catalysts.

4.3 Mechanism for anomalous growth of Pt on La-Al_2O_3 and $MgAl_2O_4$

Figure 8 shows a STEM image of the initial catalyst and after aging for 30 h at 800 ˚C in air. The image is consistent with our proposal that Pt present within the pore structure of the support is emitted in the form of PtO_2 vapor and it redeposits on the surface of the catalyst grains leading to the formation of large Pt particles. When the catalyst was aged in the form of a thin film, all of the Pt in the initial catalyst is lost to the vapor phase in a few hours (Figure 3). The gas phase PtO_2 that escapes from the catalyst support is swept away by the flowing gas when the catalyst is present in the form of a thin film. This is confirmed by the total absence of any Pt particles in the 30 hours aged sample (Figure 2 e, f). In contrast, when the catalyst is present in the form of a deep bed, we do not see any loss of Pt to the vapor phase. Therefore, the PtO_2 must be redeposited on the support.

Based on DFT calculations, Plessow et al. [19] concluded that gas phase PtO_2 does not bind to the silica support. In contrast, PtO_2 binds very strongly to step edges of ceria (111) with a heat of adsorption of 7.72 eV, which is greater than the heat of adsorption of PtO_2 on Pt (111) which has been calculated to be 7.32 eV [20]. In our previous work [14], we found that the calculated adsorption of Pt_4O_6 and $Pt_{10}O_{20}$ was too weak on CeO_2 (111) hence these species would not be stable on the Ceria (111) surface. We concluded that the ability of cerium to change oxidation state was critical for trapping PtO_2 on the surface. In the case of non-reducible supports such as La-Al_2O_3 and $MgAl_2O_4$, there may be no mechanism to trap PtO_2 coming from the gas phase. Therefore, the only sites that can bind the gas phase PtO_2 species are present on metallic Pt. The binding energy of PtO_2 on Pt (111) is 7.32 eV and Pt (111) step edges is 7.98 eV [20]. Therefore, we can expect that once a metallic Pt has formed it will continue to grow since the support does not provide any opportunities for binding the PtO_2.

Catalyst sintering is known to involve particle migration and coalescence or Ostwald ripening which involves surface diffusion of mobile species. Previous work suggests that these mechanisms may not be able to explain the phenomena observed in this study. Porsgaard et al. [12] found no movement of Pt particles when ~4 nm Pt particles on SiO_2/Si(111) were heated up to 600 ˚C in 0.5 Torr oxygen. Instead they observed a decrease in the number of particles and their height as measured by Atomic force microscopy (AFM). They concluded that Pt forms volatile species in oxygen at temperature as low as 450 ˚C leading to a decrease in the amount to Pt on the surface. Simonsen et al. [21] studied a Pt/Al_2O_3 model catalyst when exposed of 10 mbar of oxygen at 650

˚C via in situ TEM. Time-resolved images unequivocally revealed that the sintering of Pt was mediated by an Ostwald ripening process. They ruled out particle migration and coalescence as the mechanism for sintering. Due to the low pressure used in their study and the absence of a flow of gas over the surface, they did not detect any loss of Pt to the vapor phase. On the other hand, the HP-XPS involves a jet of gas impinging on the sample which Porsgaard et al. [12] felt caused the emission of Pt species. Likewise, in our experiment the flowing air sweeps away the PtO_2 emitted from the thin film model catalysts. When the sample is present in the form of a packed bed or loaded on to the ceramic crucible, the PtO_2 vapor cannot escape from the sample but tends to re-deposit. Oxide surfaces such as silica or ceria (111) do not bind the PtO_2 strongly as demonstrated by DFT calculations [12,14,20]. Therefore, at the aging temperature of 800˚C the PtO_2 will not adsorb on oxide surfaces. Only metallic Pt particles that are formed will serve as adsorption sites for the PtO_2 vapor leading to the growth of anomalously large particles.

The anomalous growth of Pt particles under these conditions is a result of the vapor phase transport [19]. This explains why abnormally large Pt particles are seen (Figure 8). Furthermore, these large particles appear to be located on the surface of the individual catalyst support particles/grains and not inside the pores, because transport of gas phase PtO_2 would be facile in the inter-particle space between catalyst grains. In a previous study of Pd sintering where the transport was exclusively through surface diffusion, we found that anomalously large particles were only seen on the perimeter of a cluster of smaller particles [22]. We conclude that an essential ingredient for abnormal particle growth must involve facile transport to the growing particle which does not happen within the pore structure of the support.

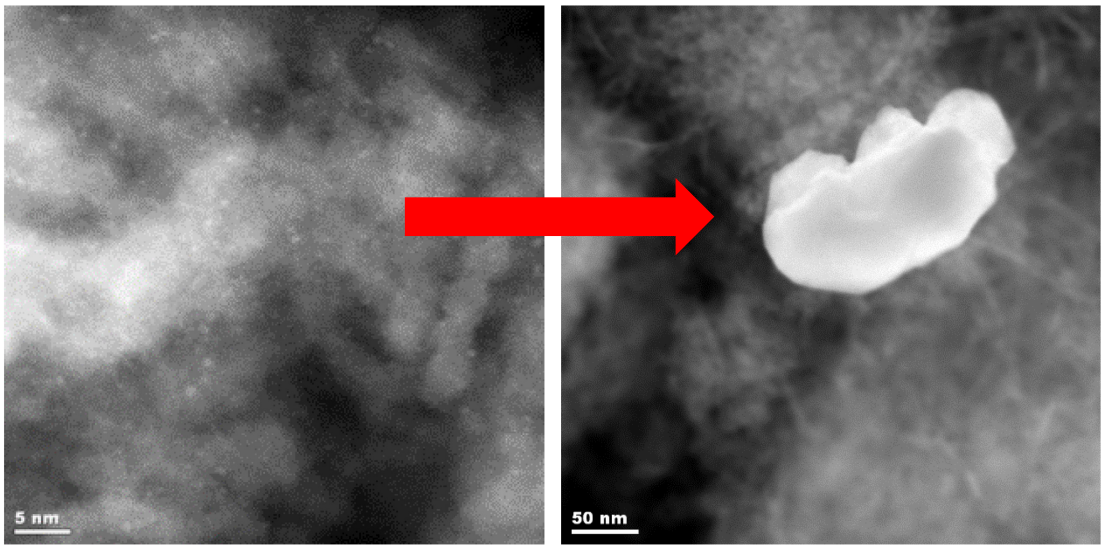

Figure 8. STEM image of (a) initial Pt/La-Al_2O_3 and b) aged 800˚C/30 h. The small particles in the initial catalysts transformed into gas phase PtO_2 which condensed into abnormally large Pt particles.

It was reported by Li et al. [10] that Pt particles are stabilized on Pt/$MgAl_2O_4$ in contrast to Pt on commercial Al_2O_3. In this work, however, we do not find any difference between these two supports. The loss of Pt to the vapor phase is equally rapid (Figure 3) and large particles are found after aging at 800 °C on both supports (Figure 5) and they show similar CO oxidation reactivity after 30 h aging at 800 °C in air (Figure 7b). It is clear that the large particles were non-existent initially, and the rates of mass transfer for Pt are rapid enough for the formation of large particles seen in these catalysts. Earlier reports indicating the growth of Pt particles via vapor-phase transport of PtO_2 on supported catalysts [3,19,23] are consistent with our observations. The stochastic nature of nucleation, and the limited number of nucleation sites for Pt particles help explain why the few particles that are formed continue to grow, fed by the presence of PtO_2 vapor, leading to abnormally large Pt particles when aged at 800 °C in air.

6. Conclusions

We observed a loss of Pt from Pt/La-Al_2O_3 and Pt/$MgAl_2O_4$ when the catalyst was present in the form of a thin film. The loss of Pt is attributed to the formation of volatile species PtO_2 via the

reaction of Pt with oxygen at elevated temperatures. STEM images of initial catalysts $Pt/MgAl_2O_4$ and $Pt/La\text{-}Al_2O_3$ show small and homogenously distributed nanometer Pt particles. After aging the catalyst in the form of a thin film, all the Pt is lost because it is swept away by the flowing air. No loss of Pt is seen from Pt/CeO_2 because the Pt is present as Pt^{2+} bound to four oxygen atoms. Similar measurements were carried out with the powder catalyst placed in a ceramic crucible boat. With this geometry, there was no loss of Pt because the gas-phase PtO_2 condensed within the bed to form large Pt particles. Due to the inability of PtO_2 to bind strongly to $MgAl_2O_4$ and $La\text{-}Al_2O_3$, metallic platinum provides the only strong binding sites to capture gas phase PtO_2. This leads to the growth of few particles that continue to grow, fed by the high vapor-phase concentration of PtO_2. This work shows the importance of vapor-phase transport for the observed anomalous growth patterns. Our work was directed towards understanding phenomena that occur under lean accelerated diesel catalyst aging conditions, such as those specified by the USDRIVE Low Temperature aftertreatment (LTAT) test protocol [1]. We have previously demonstrated, as have other researchers, that under reducing conditions atomically dispersed Pt transforms into nanoparticles [17]. The transformation from nanoparticles into atomically dispersed Pt is reversible on ceria support as shown by Ganzler et al. [24]. Therefore, the results presented here are also relevant to Pt/CeO_2 subjected to reducing conditions.

Acknowledgements

The research was supported by supported by NSF GOALI grant CBET-1707127 and General Motors Global R&D. Additional funding from the U.S. Department of Energy grant DE-FG02-05ER15712 is also acknowledged.

References

[1] USDRIVE, Aftertreatment Protocols for Catalyst Test Characterization and Performance: Evaluation Low-Temperature Oxidation Catalyst Test Protocol 2015, (2015) https://cleers.org/wp-content/uploads/2015_LTAT-Oxidation-Catalyst-Characterization-Protocol.pdf.

[2] G.W. Graham, H.W. Jen, O. Ezekoye, R.J. Kudla, W. Chun, X.Q. Pan, R.W. McCabe,

Effect of alloy composition on dispersion stability and catalytic activity for NO oxidation over alumina-supported Pt-Pd catalysts, Catal. Letters. 116 (2007) 1–8.

[3] P.J.F. Harris, E.D. Boyes, J.A. Cairns, The sintering of an alumina-supported platinum catalyst studied by transmission electron microscopy, J. Catal. 82 (1983) 127–146.

[4] P. Wynblatt, Particle Growth in Model Supported Metal Catalysts-II. Comparison of Experiment with Theory, Acta Metall. 24 (1976) 1175–1182.

[5] C.B. Alcock, G.W. Hooper, Thermodynamics of the Gaseous Oxides of the Platinum-Group Metals, Proc. R. Soc. A Math. Phys. Eng. Sci. 254 (1960) 551–561.

[6] J. Jones, H. Xiong, A.T. DeLaRiva, E.J. Peterson, H. Pham, S.R. Challa, G. Qi, S. Oh, M.H. Wiebenga, X.I.P. Hernández, Y. Wang, A.K. Datye, Thermally Stable Single-Atom Platinum-on-Ceria Catalysts via Atom Trapping, Science. 353 (2016) 150–154.

[7] H. Xiong, E. Peterson, G. Qi, A.K. Datye, Trapping mobile Pt species by PdO in diesel oxidation catalysts: Smaller is better, Catal. Today. 272 (2016) 80–86.

[8] C. Carrillo, A. DeLaRiva, H. Xiong, E.J. Peterson, M.N. Spilde, D. Kunwar, R.S. Goeke, M. Wiebenga, S.H. Oh, G. Qi, S.R. Challa, A.K. Datye, Regenerative trapping: How Pd improves the durability of Pt diesel oxidation catalysts, Appl. Catal. B Environ. 218 (2017) 581–590.

[9] E. Mamontov, T. Egami, R. Brezny, M. Koranne, S. Tyagi, Lattice Defects and Oxygen Storage Capacity of Nanocrystalline Ceria and Ceria-Zirconia, J. Phys. Chem. B. 104 (2000) 11110–11116.

[10] W.Z. Li, L. Kovarik, D. Mei, J. Liu, Y. Wang, C.H.F. Peden, Stable platinum nanoparticles on specific MgAl 2 O 4 spinel facets at high temperatures in oxidizing atmospheres, Nat. Commun. 4 (2013) 1–8.

[11] H. Wang, J. Dong, L.F. Allard, S. Lee, S. Oh, J. Wang, W. Li, Single-site Pt /La-Al_2O_3 stabilized by barium as an active and stable catalyst in purifying CO and C_3H_6 emissions, Appl. Catal. B Environ. 244 (2019) 327–339.

[12] A. X, S. Porsgaard, L.R. Merte, L.K. Ono, F. Behafarid, J. Matos, S. Helveg, M. Salmeron,

B.R. Cuenya, F. Besenbacher, Stability of Platinum Nanoparticles Photoelectron Spectroscopy Study, ACS NANO. (2012) 10743–10749.

[13] G.C. Fryburg, H.M. Petrus, Kinetics of the Oxidation of Platinum, J. Electrochem. Soc. (1961) 496–503.

[14] D. Kunwar, S. Zhou, A. De La Riva, E. Peterson, H. Xiong, X.I. Pereira Hernandez, S.C. Purdy, R. ter Veen, H.H. Brongersma, J.T. Miller, H. Hashiguchi, L. Kovarik, S. Lin, H. Guo, Y. Wang, A. Datye, Stabilizing High Metal Loadings of Thermally Stable Platinum Single Atoms on an Industrial Catalyst Support, ACS Catal. 9 (2019) 3978-3990.

[15] F. Dvořák, M.F. Camellone, A. Tovt, N. Tran, F.R. Negreiros, M. Vorokhta, T. Skála, I. Matolínová, J. Mysliveček, V. Matolín, S. Fabris, Creating Single-Atom Pt-Ceria Catalysts by Surface Step Decoration, Nat. Commun. 7 (2016) 1–8.

[16] Y. Nagai, T. Hirabayashi, K. Dohmae, N. Takagi, T. Minami, H. Shinjoh, S. Matsumoto, Sintering inhibition mechanism of platinum supported on ceria-based oxide and Pt-oxide-support interaction, J. Catal. 242 (2006) 103–109.

[17] X.I. Pereira-Hernández, A. DeLaRiva, V. Muravev, D. Kunwar, H. Xiong, B. Sudduth, M. Engelhard, L. Kovarik, E.J.M. Hensen, Y. Wang, A.K. Datye, Tuning Pt-CeO2 interactions by high-temperature vapor-phase synthesis for improved reducibility of lattice oxygen, Nat. Commun. 10 (2019) 1358.

[18] K. Leistner, C. Gonzalez, A. Kumar, K. Kamasamudram, L. Olsson, Applied Catalysis B : Environmental Volatilisation and subsequent deposition of platinum oxides from diesel oxidation catalysts, Appl. Catal. B Environ. 241 (2019) 338–350.

[19] P.N. Plessow, F. Abild-Pedersen, Sintering of Pt Nanoparticles via Volatile PtO2: Simulation and Comparison with Experiments, ACS Catal. 6 (2016) 7098–7108.

[20] X. Wang, J.A. van Bokhoven, D. Palagin, Ostwald Ripening versus Single Atom Trapping: Towards Understanding Platinum Particle Sintering, Phys. Chem. Chem. Phys. 19 (2017) 30513–30519.

[21] S.B. Simonsen, I. Chorkendorff, S. Dahl, M. Skoglundh, Direct Observations of Oxygen-induced Platinum Nanoparticle Ripening Studied by In Situ TEM, J. Am. Chem. Soc.

(2010) 7968–7975.

[22] A.D. Benavidez, L. Kovarik, A. Genc, N. Agrawal, E.M. Larsson, T.W. Hansen, A.M. Karim, A.K. Datye, Environmental transmission electron microscopy study of the origins of anomalous particle size distributions in supported metal catalysts, ACS Catal. 2 (2012) 2349–2356.

[23] P. Wynblatt.and N. A. Gjostein, Particle Growth in Model Supported Metal Catalysis-I. Theory, Acta Metall. (1976) 1165–1174.

[24] A. Gänzler, M. Casapu, F. Maurer, H. Störmer, D. Gerthsen, G. Ferré, P. Vernoux, B. Bornmann, R. Frahm, V. Murzin, M. Nachtegaal, M. Votsmeier, J.-D. Grunwaldt, Tuning the Pt/CeO_2-Interface by In Situ Variation of the Pt Particle Size, ACS Catal. 8 (2018) 4800–4811.